Supporting Information

Thickness determination. The thickness for AuNP-PVP films was measured to be 70 ± 7 nm,[27] by an atomic force microscope (AFM) (Veeco Dimension 3100, Vecco, Plainview, NY, USA). Surface profilometer readings (DekTak, Bruker, Billerica, MA, USA) and estimation from optical spectra by Beer-Lambert law consistently measured PVP film thicknesses of sub-100 nm. Thickness measurements by cross-sectional SEM (Philips XL40, FEI; Hillsboro, OR, USA) were also performed. However, it was not possible to distinguish the PVP film from its underlying BK-7 glass substrate because of charging concomitant with low Z-contrast between the two materials. Additionally, SEM could not clearly distinguish the three-dimensional distribution of AuNP because of (i) inability to extract secondary electrons from AuNP immersed within the insulative PVP, (ii) relatively small size of the 16 nm AuNP as compared to the 6 nm resolution of the SEM, and (iii) difficulty in distinguishing boundaries of the 70 nm PVP film. Figure S1 illustrates difficulty in SEM analysis of these samples. Briefly, a sample was scratched at the edge with a razor blade, tilted at 60º in the SEM, and imaged with 10 kV to minimize charging. The LHS micrograph shows the scratch in the AuNP-PVP film with the exposed BK7 edge facing upwards. Specks in the PVP were dust, rather than AuNP which are shown in Figure 1 insets. Peeling of the PVP was apparent, but cumulative effects of charging and low spatial dimensionality precluded an accurate measurement of thickness based on these features. The RHS micrograph zooms in on the Au-PVP and BK7 edge boundary in between the scratches and peeling. Poor resolution results from differences in charging between the BK7 and PVP, which consequently made astigmatism corrections difficult in the absence of conductive media. Note the scale of the RHS micrograph, which is three orders-of-magnitude greater than the 70 nm PVP film thickness estimation by AFM.

Overall, the SEM images did not clearly resolve PVP film thickness or AuNP embedded three-dimensionally within the PVP.

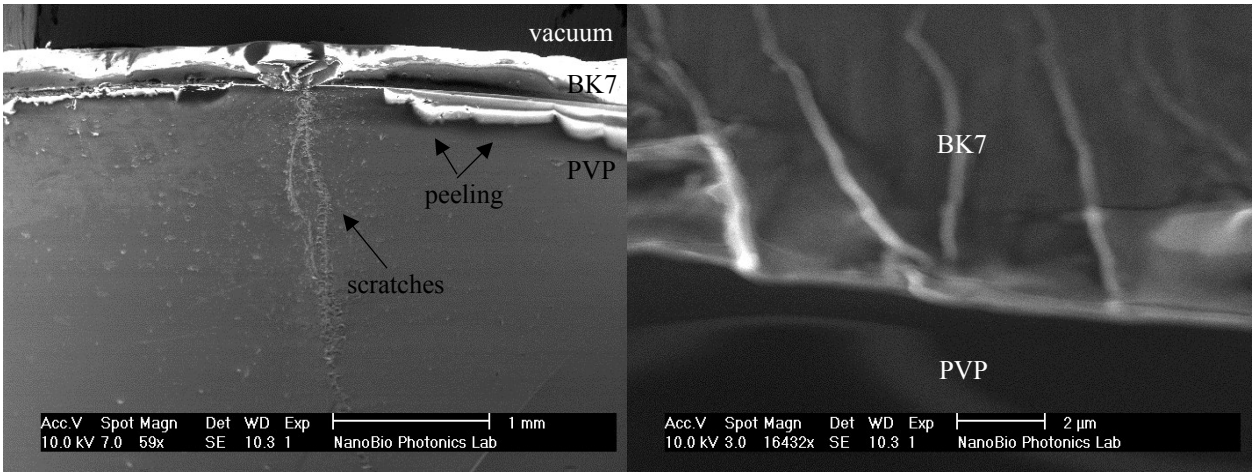

Figure S1. Tilted SEM micrographs of a representative AuNP-PVP sample at increasing magnification.

Maxwell Garnett Effective Medium Theory. From Maxwell Garnett relations, measurable geometric optical properties may be approximated from dielectric functions accounting for components of constituents of an effective medium based upon the number of inclusions per unit volume, N_j, in a material j, that has a uniform, microscopic polarizability α_j. These values are then used to determine the complex permittivity ε_{eff} of a macroscopic, homogeneous, isotropic effective medium specified by the Clausius-Mossotti relation[44]

$$\frac{\varepsilon_{eff} - 1}{\varepsilon_{eff} + 2} = \frac{4\pi}{3}\sum_j N_j \alpha_j \qquad (1)$$

where $\varepsilon_{eff} = \varepsilon_{1,eff} + i\varepsilon_{2,eff}$. With a spherical inclusion i of radius r, the polarizability is defined classically in terms of its complex dielectric function, ε_i, given as[45]

$$\alpha_i = \left(\frac{\varepsilon_i - 1}{\varepsilon_i + 2}\right) r^3 \tag{2}$$

Given a material containing only uniform spherical inclusions, equation 2 may be substituted into equation 1. With this substitution, a spherical inclusion volume fraction, $\delta_i = N_i \frac{4}{3}\pi r^3$ must be included yielding

$$\frac{\varepsilon_{eff} - 1}{\varepsilon_{eff} + 2} = \delta_i \left(\frac{\varepsilon_i - 1}{\varepsilon_i + 2}\right) \tag{3}$$

As the inclusions are embedded in a material the relative permittivity of the material, ε_m, must be accounted for, making equation 3[44]

$$\frac{\varepsilon_{eff} - \varepsilon_m}{\varepsilon_{eff} + 2\varepsilon_m} = \delta_i \left(\frac{\varepsilon_i - \varepsilon_m}{\varepsilon_i + 2\varepsilon_m}\right) \tag{4}$$

Equation 4 simplifies to equation 3 when the spherical inclusions are in a vacuum, $\varepsilon_m = 1$. By then solving for ε_{eff} in equation 4, the Maxwell Garnett equation for effective relative permittivity is[31]

$$\varepsilon_{eff} = \varepsilon_m \left(\frac{2\delta_i(\varepsilon_i - \varepsilon_m) + \varepsilon_i + 2\varepsilon_m}{2\varepsilon_m + \varepsilon_i + \delta_i(\varepsilon_m - \varepsilon_{i)}}\right) \tag{5}$$

The real, ε_1, and imaginary, ε_2, components of equation 5, the real part of the refractive index (RI), n_{eff}, and the corresponding absorption coefficient, k_{eff}, are[46]

$$n_{eff} = \frac{1}{\sqrt{2}}(\varepsilon_{1,eff} + (\varepsilon_{1,eff}{}^2 + \varepsilon_{2,eff}{}^2)^{1/2})^{1/2} \tag{6a}$$

$$k_{eff} = \frac{1}{\sqrt{2}}(-\varepsilon_{1,eff} + (\varepsilon_{1,eff}{}^2 + \varepsilon_{2,eff}{}^2)^{1/2})^{1/2} \tag{6b}$$

Given the real part of the refractive index and absorbance coefficient, the geometric optical transmission, *T*, and reflection, *R*, for an effective medium film of thickness *l* where a wavelength of light λ, in a vacuum, is incident on is calculated using equations 6a and 6b via[46]

$$R = \frac{(n_{eff} - 1)^2 + {k_{eff}}^2}{(n_{eff} + 1)^2 + {k_{eff}}^2} \tag{7}$$

$$T = \frac{(1 - R)^2 e^{-4\pi k_{eff} l/\lambda}}{1 - (R^2 e^{-8\pi k_{eff} l/\lambda})} \tag{8}$$

From equation 8, the experimental absorbance may be calculated via $A = -log_{10} T$. For Au and PVP, complex relative permittivity values of -4.856+2.123i and 2.342+0.007i at 532 nm were respectively used. The RI for PDMS (Dow Corning, Sylgard) was 1.42.[49]

Coupled Dipole Approximation. In CDA,[22,23] approximations, the i^{th} nanoparticle in an ensemble[52,53] is treated as a single dipole with a polarization proportional to the local electric field given by

$$P_i = \alpha_i E_{tot}(r_i)$$

where α is a frequency-dependent polarizability and E_{tot} sums incident (E_o) and scattered fields (E_{lat}). Polarizabilities of particles are also available from analytical formulae,[52] which limit approximations from higher order modes[53] and computational results.[14,54] Using matrix inversion, the resulting equations were solved for each particle in a user-defined array.[55,56] Given a finite number of dipoles, each dipole pair was calculated via superposition to calculate the polarization vector, P_i, at each dipole. Simulations were analyzed with 16 nm diameter spheres in media refractive indices for PVP of 1.53, and varying angles of incident radiation.[58] Using a square

150x150 grid (90,601 dipoles) with a grating constant double the Wigner-Seitz radius, defined as $r_{W\text{-}S} = r_p(\rho_{Au}/x)^{1/3} = (3V/4\pi N)^{1/3}$, where r_p is the particle radius, ρ_{Au} is the density of gold (19.3 g/cm^3), *x* is gold mass per cubic centimeter of host media, V is the media volume, and N is the number of particles.

Gold Nanoparticle Specifications. AuNP (Econix Dried, Nanocomposix, San Diego, CA, USA) were reported to have a standard deviation of 2.4 nm. The thickness of the PVP coating was reported to be less than or equal to 4.4 nm, with a coefficient of variation of 15.3%. Spectra of AuNP nanoparticles is shown in Figure S2.

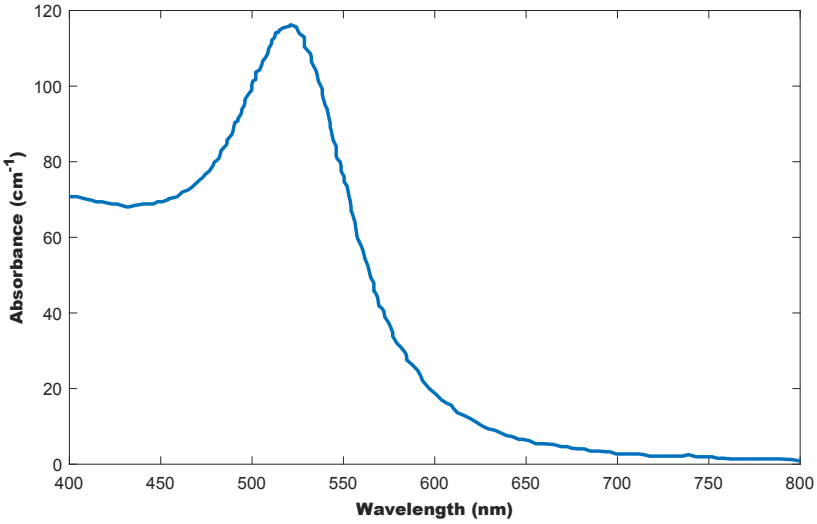

Figure S2. Measured optical spectra of AuNP in water.

Optical Setup: Resonant irradiation from a fiber-coupled 532 nm diode-pumped solid state laser (MXL-FN-532, CNI, Changchung, CN), continuous wavelength and greater than 100:1 polarization ratio in the horizontal, was collimated (10.90 mm focal length, 0.25 NA) (F220SMA-A, Thorlabs, Newton, New Jersey, USA) and passed through a ground glass diffuser (DGUV10-

1500, Thorlabs, Newton, NJ, USA) prior to focusing onto the sample by a lens pair. The ground glass surface of the diffuser re-distributed the laser power profile to that of a Gaussian distribution, shown in Figure S3. The lens pair consisted of two lenses: (i) a 60 mm focal length, 0.61 NA (ACL7560U, Thorlabs, Newton, New Jersey, USA) lens captured diffuse light for an infinity space and (ii) a 16 mm focal length, 0.79 NA (ACL25416U, Thorlabs, Newton, New Jersey, USA) to focus the Gaussian-distributed power onto the sample, 10 mm away from previous lens, at a 1.2 ±0.13 mm D4σ focal spot size estimated using Vernier calipers (N=20). The 1.2 mm spot size was measured at the focal point of the beam where each sample was placed.

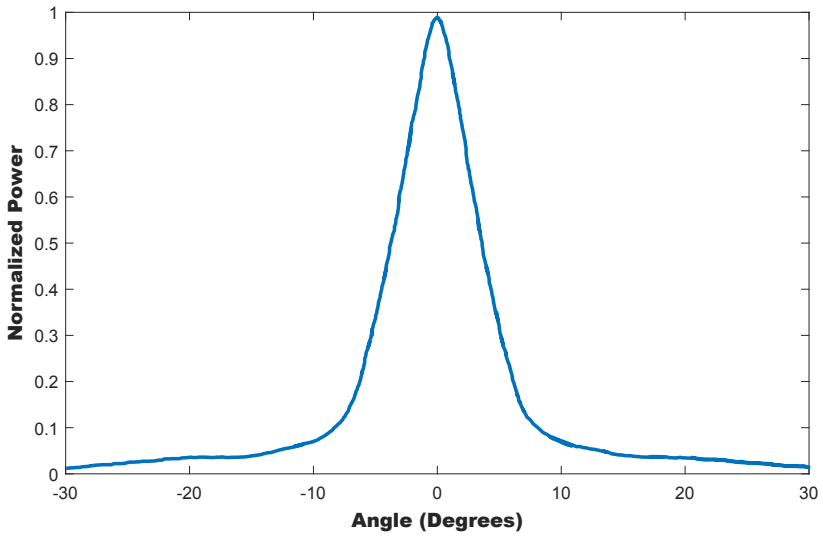

Figure S3: Power Distribution of Ground Glass Diffuser.

Wigner-Seitz Radius: Values of Wigner Seitz radius calculated for corresponding AuNP concentrations are summarized in the following table.

AuNP Concentration (x10^{15} NP/cm^3)	Wigner-Seitz Radius (nm)
1.01	68

1.69	55
2.53	48
3.37	44
5.06	38

Thermography capture and analysis. Thermal micrographs were captured at 10 Hz over a 180 s time interval: 90 s of heating (including 3 s of ambient) with the laser on and 90 s of cooling with the laser off. Thermal micrographs were analyzed via MATLAB program using a circular region of interest (ROI) encompassing solely the laser spot for each sample, shown in Figure S4 (a). Pixel values within the ROI were averaged together, to give temperature values used for the analysis of data. Plots of temperature within the ROI versus time extracted from these images for each sample are shown in Figure S4(b). The change in equilibrium peak temperature for control (0.00), 1.01, 2.53, and 5.06 x 10^{15} NP/cm^3 are shown in Figure S4(c). A plot of peak temperature change vs. nanoparticle concentration data does not account for effects of irradiated spot size or film thickness to facilitate direct comparison with both measured and simulated optical extinction. Power of the laser was recorded before and after each trial to ensure power did not fluctuate beyond a 10 mW threshold during data capture. Pixel resolution was 238 µm.

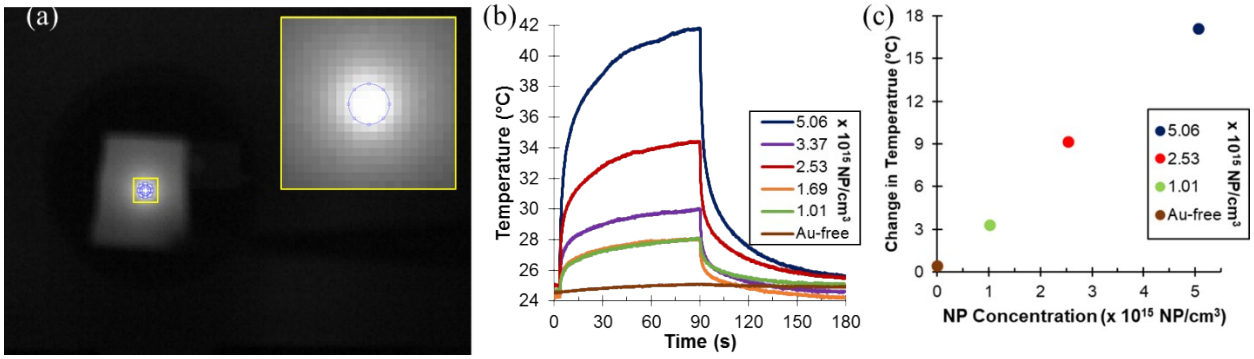

Figure S4. (a) Example of MATLAB program with circular region of interest for 5.06 x 10^{15} NP/cm^3 AuNP concentration sample. Outlined yellow box in upper right corner is zoomed view indicating actual pixels used for analysis. Region of interest is centered around most illuminated pixels, i.e. where the laser spot is hitting the sample. (b) Average temperature within the region of interest against time, with varying concentrations of AuNP. (c) Peak change in temperature values for control (0.00), 1.01, 2.53, and 5.06 x 10^{15} NP/cm^3 samples. Error for change in temperature was determined by the standard deviation, and is obscured by the marker of each data point.

Laser-induced damage. Photodamage was evident in SEM analysis of the 3.37 x 10^{15} NP/cm^3 film where the laser was incident. Figure S4 shows two SEM micrographs of this sample at (a) the irradiated area and (b) a representative un-irradiated area near the sample periphery. SEM imaging conditions were top-down (normal incidence) orientation, 10 kV. In addition to the 16 nm AuNP observable in each, image (a) also featured "crater-like" features ca. 75-100 nm in size. Each "crater" was composed of eccentric circles. Darker of the two circles could have been the underlying, insulative BK7 support glass. Origin of the darker lighter of the two circles is unknown. Thermal damage resulting from irradiation of AuNP is one possibility. Cross section images of the films are shown in Figure S1.

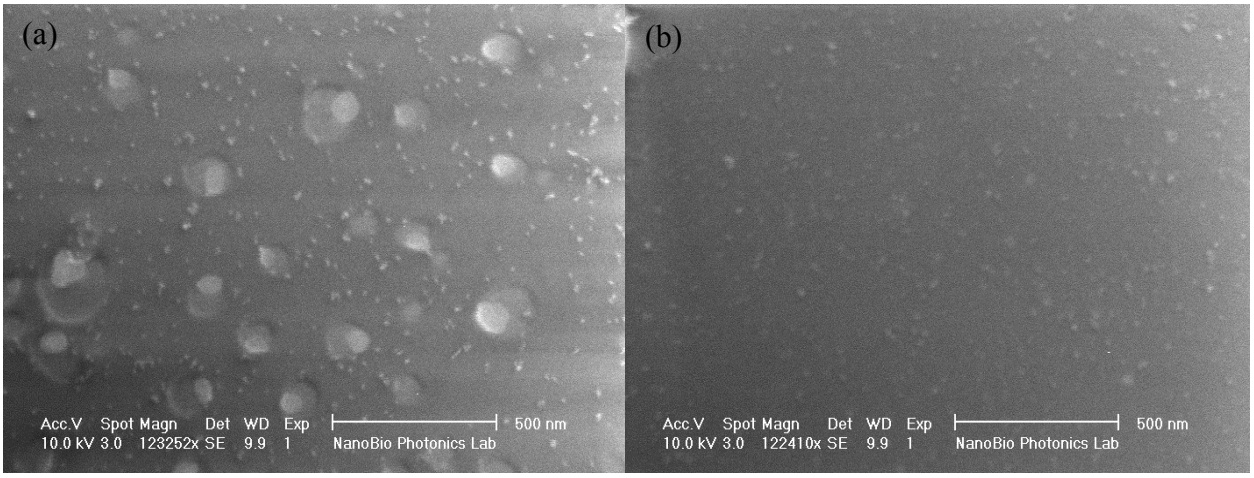

Figure S5. SEM micrographs taken at normal incidence of the 3.37 x 10^{15} NP/cm^3 sample (a) within the laser spot and (b) outside the laser spot. Accelerating voltage was 10 kV.

Finite Element Analysis model geometry. The model geometry used for the thermal simulations using Finite Element Analysis (COMSOL) is shown in Scheme S1. The 70 nm thick AuNP-PVP layer and adjacent 500 micron thick glass layer are both assumed to be 10 mm x 10 mm. The 1.2 mm heat source (red) estimating plasmonic absorption is centered within the AuNP-PVP layer only. Values for density and heat capacity, 1380 (19300) kg/m^3 and 1605 (129 W/mK), respectively, for PVP (gold) were used to calculate volume fraction weighted values, shown in Table S1, for use in the thermal model. Density and heat capacity values used for glass were 2210 kg/m^3 and 1.1 W/mK, respectively. Relative permittivity (dielectric function) of Au and PVP (values given above) were used to determine the fraction of incident power absorbed via EMT and CDA descriptions as detailed above. Relative permittivity (dielectric function) was not used in the thermal model.

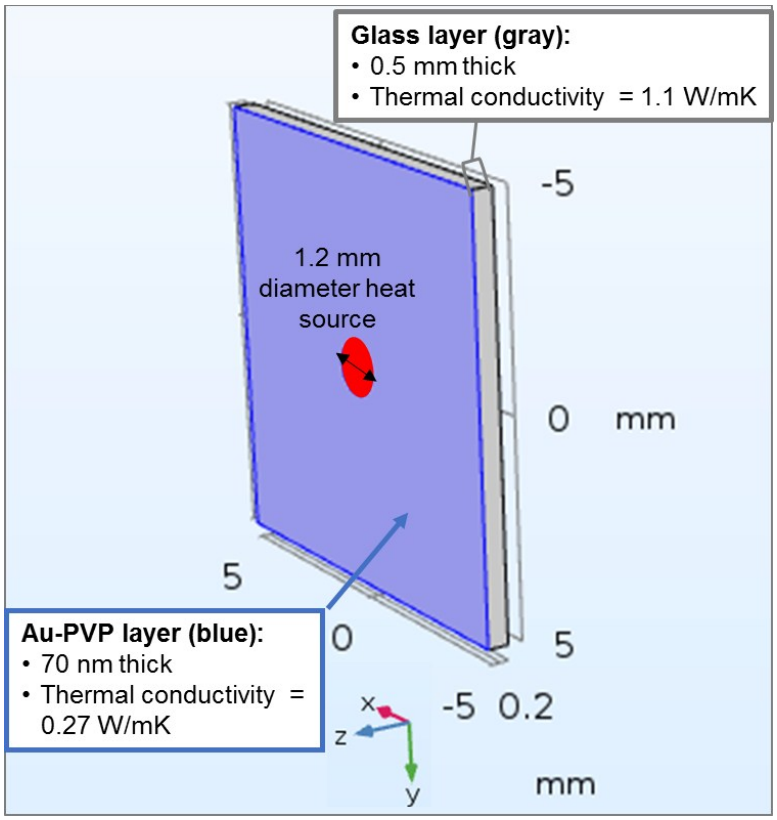

Scheme S1. Schematic of the model geometry used to estimate thermal response.

Volume Fraction Au	Volume Fraction PVP	Au density (kg/m^3)	PVP density (kg/m^3)	Au heat capacity (J/kgK)	PVP heat capacity (J/kgK)	Weighted density (kg/m^3)	Weighted heat capacity (J/kgK)
0.002	0.998	19300	1380	130	1605	1419	1602
0.004	0.996	19300	1380	130	1605	1445	1600
0.005	0.995	19300	1380	130	1605	1477	1597
0.007	0.993	19300	1380	130	1605	1509	1594

Table S1. Volume fraction averaged values for density and heat capacity for AuNP-PVP composites

Comparison of Measured and Simulated Optically Extinguished Power with Temperature Profiles. Consideration of reflection values for AuNP-PVP films decreased the measured optically extinguished power across all samples, leading to a greater agreement between measured and FEA

fitted powers. Figure S6 (a) shows the measured optically extinguished power with (green-filled diamond) and without (orange-filled triangle) reflection values taken into account in relation to FEA fitted power (blue-open circles). Accounting for reflection improved agreement between measured and FEA-fitted power by 181% to 25%. Specifically, agreement increased 181, 202, 42, and 25%, respectively, as AuNP concentration increased.

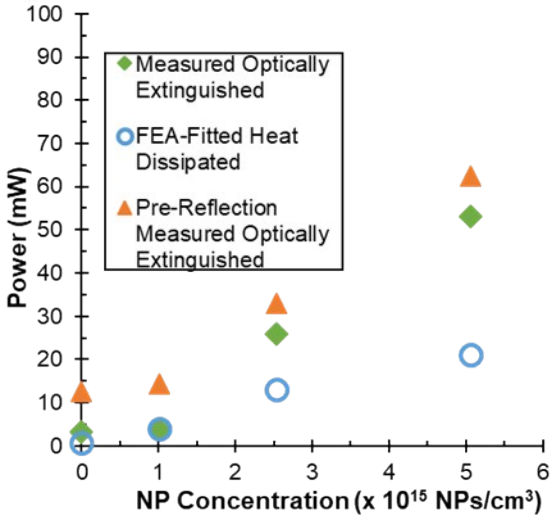

Figure S6. Optically extinguished power before reflection was accounted (filled orange triangles), after reflection was accounted (filled green diamonds), and FEA-fitted dissipated thermal power based on measured temperature distribution (open blue circles) as a function of AuNP concentration. Error bars in optically extinguished power was calculated as the difference of the upper/lower measured power with average power recorded across all trials for each sample. Error in FEA-fitted heat dissipated power (within size of the symbol) was based on two alternative fitting parameters. Calculated error for measured optically extinguished power and FEA-fitted power was determined by $\sigma_{H,L} = |P_{H,L} - P_{average}|$, with H,L corresponding to highest and lowest measured powers, and $P_{average}$ is the average of the high and low measured powers, for each sample.